Principal Curves for Tree Topology Retrieval from TLS Data

Anita Schilling[1], Anja Schmidt[1], Hans-Gerd Maas[1]

[1]Institute of Photogrammetry and Remote Sensing, Technische Universität Dresden,
anita.schilling@tu-dresden.de, anja.schmidt@tu-dresden.de,
hans-gerd.maas@tu-dresden.de

Paper Number: 042

Abstract

Reconstruction of a tree's topological and geometrical structure from terrestrial laser scanner point clouds is a fundamental step in order to gain insight into plant processes like water interception or light absorption. We propose to utilize principal curves as a novel approach to retrieve skeletal structures from TLS data sets. A principal curve is a polygonal line that traces the shape of a 3D point cloud by minimizing the expected squared distance to the given data set. Experiments are conducted to assess the feasibility and benefit of applying principal curves to single tree data sets. A previous segmentation of each tree into its phyto-elements is necessary and has been performed manually for simplicity. However, instead of introducing an arbitrary neighborhood structure like a voxel grid or graph, we propose to exploit the implicit neighborhood structure provided by each single TLS scan to facilitate data processing. Our results show that principal curves are an excellent tool for the retrieval of skeletal structures from point clouds and a fully automatic preprocessing should be aimed at in the future.

1. Introduction

Terrestrial laser scanners (TLS) have proven to be invaluable for capturing plant geometry data as 3D point cloud in a very efficient and precise way. However, the diversity in tree vegetation geometry and appearance makes it difficult to derive general constraints for tree reconstruction. Further complicating factors are technique-related effects during scanning like data gaps caused by occlusions, especially self-occlusions of branches in the tree crown, and artifacts due to wind movements. Moreover, the number of measured 3D points has a significant impact on the processing performance and the quality of results. In essence, processing scanned 3D point clouds with the objective to retrieve a skeletal representation of a tree's spatial structure is still a rather challenging task.

A common approach to deal with unorganized 3D point sets is the utilization of a voxel space representation of the data. (Gorte and Pfeifer 2004; Gorte and Winterhalder 2004) employed connected component labeling and mathematical morphology to carve out the skeleton of a tree from a voxel space representation. In (Gorte 2006), the procedure was improved further by incorporating Dijkstra's shortest path algorithm (Dijkstra 1959). A similar method was presented in (Gatziolis *et al.* 2010). A graph-reduction approach for skeleton extraction was introduced in (Bucksch 2011) mapping the point cloud onto an octree structure, which is then subjected to a set of fixed rules. However, the procedure tends to cause loops in the skeleton during graph processing and is computationally expensive. Recently, (Schilling *et al.* 2012) presented a method to retrieve a spatial tree representation utilizing Depth-First Search on the voxel representation of single tree point clouds. In general, voxel space approaches have the advantage of providing a fixed neighborhood structure that the raw 3D point cloud in most cases lacks. Nevertheless, methods based on voxel grids are usually hard to handle regarding the steering parameters and processing rules, and are computationally demanding.

In contrast, the raw 3D point set was used in (Livny *et al.* 2010) to create a weighted graph from which skeletal structures were retrieved by Dijkstra's algorithm. A similar approach was presented in (Côté *et al.* 2011), where intensity information was also taken into account, and

(Xu *et al.* 2007). In (Preuksakarn *et al.* 2010), the tree skeleton was retrieved by application of a point set contraction algorithm (Giannitrapani and Murino 1999). A probabilistic approach using general knowledge to guide a tree skeleton reconstruction process with iterative cylinder fitting was introduced in (Binney and Sukhatme 2009). In (Yan *et al.* 2009), an adjacency graph was built between point clusters previously established by repetitive k-means and fitting of minimum boundary cylinders. Furthermore, a method segmenting the range image of the point cloud based on local curvature estimates is detailed in (Dai *et al.* 2010). Subsequently, the skeleton is recovered from bins of clusters resulting from a previous region growing procedure. A similar approach utilizing principal curvature is presented in (Cheng *et al.* 2006). Since point clouds acquired by powerful TLS such as the Z+F Imager 5006i are rather large in size, computation of a nearest neighbor graph and application of graph algorithms becomes infeasible. Furthermore, the problem of occlusions, artifacts, and larger data gaps still remains.

In this paper, we propose a novel approach to retrieve skeletal representations of trees from 3D point clouds on the basis of principal curves. A principal curve is a polygonal line that provides a compact summary of the point distribution of the 3D data and can be computed automatically. For this reason, principal curves are an obvious choice to trace point subsets representing tree branches; but to our knowledge, they have not been applied to TLS data before. Consequently, we present experiments that have been conducted in order to assess the feasibility of utilizing principal curves on TLS data.

The paper is organized as follows: First, principal curves and their computation scheme is introduced. Second, the study site and data preprocessing are detailed. Subsequently, a discussion of the results is presented. The paper closes with a summary of the conducted work in the conclusion.

2. Principal Curves

A 3D point set measured by a terrestrial laser scanner is a noisy point sampling of the geometry of a real-world object. If information on the object's geometry is available, its recovery from the 3D point set becomes feasible. In case of a 3D point set representing a cylindrical object, fitting a 3D center line by means of principal component analysis (e.g. (Jolliffe 2002)) is a trivial task. However, if the object resembles a tube, as is commonly observed at tree branches, recovering the underlying space curve from the 3D point set is far more difficult. If a model for the 3D curve cannot be determined in advance, methods based on Ransac (Fischler and Bolles 1981) cannot be applied because they require a known curve model to assess the error of the data points during computation.

In order to recover the underlying 3D curve from a 3D point set representing a tree branch or trunk, we propose the application of principal curves as defined in (Kégl *et al.* 2000): A principal curve is a polygonal line that traces the shape of a 3D point cloud by minimizing the expected squared distance to the given data set. In case of a 3D point set of a branch, it passes along the center of the branch. As detailed in (Kégl 1999; Kégl *et al.* 2000), the principal curve can be retrieved automatically from the 3D point set P with n denoting the number of data points. The first principal component of a subset of P is utilized as an initial line estimate. Successively, the algorithm alternates in an inner loop between a repartitioning of the data points according to their projections onto the curve, and an optimization computation of the curve vertices. After completing the inner loop, a new vertex is added to the curve and the inner loop is repeated. The computation terminates when a criterion $c(n, \Delta f_{k,n})$ is fulfilled, which incorporates the number of curve segments k and an error measure $\Delta f_{k,n}$ assessing the curve node positions in relation to their corresponding point subsets. The resulting polygonal line $f_{k,n}$ provides a compact description of the spatial distribution of the 3D point set P. Algorithm 1 provides an outline of the computation scheme.

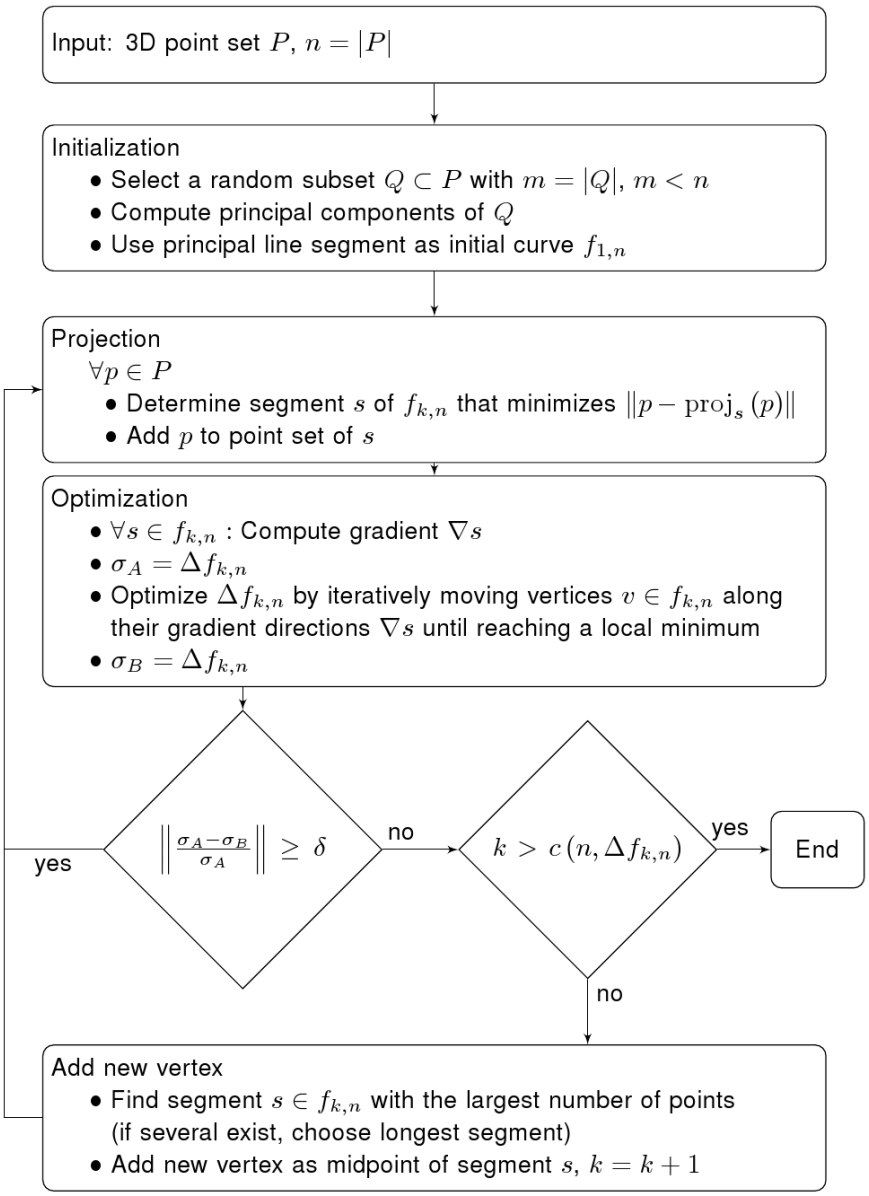

Algorithm 1: Principal curves computation scheme based on (Kégl *et al.* 2000). δ denotes a predefined threshold of relative change.

3. Methods

3.1 Study Site and Data Processing

The study site comprises a plain birch stand (Betula pendula) on an area of ca. 1.3 ha (160 m × 80 m) near Wilmsdorf, Germany. The birch stand has been scanned in leafless condition using the TLS Z+F Imager 5006i with a field of view of 360° in horizontal, 310° in vertical direction and an angular resolution of 0.018°; for TLS specifications see (Zoller+Fröhlich 2009). For each independent scan, the data is provided similar to a range image. But here, each pixel of the image matrix represents a data tuple t in the form $t = (p_X, p_Y, p_Z, d, i)$, offering the 3D coordinates $(p_X, p_Y, p_Z) \in \mathbb{R}^3$ as well as the intensity value $i \in [0..1]$ in addition to each measured range $d \in \mathbb{R}^+$. If the measurement has failed at a particular pixel then an empty tuple $t_e = (0,0,0,0,0)$ has been stored. Arranging all of one scan's data in the same fashion as its range image makes each measured point readily accessible by its 2D coordinates in the image matrix. Hence, introducing an arbitrary neighborhood structure like a voxel grid or graph is not required.

The particular scan itself provides an implicit neighborhood structure, which can be directly exploited and facilitates general data processing as image processing methods can be applied to the 3D data as well. Another advantage is the possibility to visualize all data aspects of the scan within the image matrix, which provides a better and intuitive insight into the data set.

From the obtained scans, a set of 10 trees has been selected in $7.25\,m$ to $20.57\,m$ distance from the scanner position and exported as follows: All pixels of the original image matrix are checked and those, which hold 3D coordinates that are further away from the predefined tree position in the XY plane than $3\,m$, are replaced by empty tuples. Subsequently, the image matrix is clipped to the size of the 2D bounding box of the remaining non-empty tuples. For each tree, the result is a cutout of the original image matrix of the single-view scan, as shown in figure 1a.

Since the result of the principle curve computation is a single polygonal line, each tree has to be segmented into disjoint point sets denoting branches and the trunk. The result of this preprocessing step is a new image matrix, where each tuple $\hat{t} = (p_X, p_Y, p_Z, d, i, l)$ has an additional element $l \in \mathbb{N}^+$ denoting the point subset it belongs to. If the pixel contains an empty tuple, the label $l = 0$ is assigned, which denotes *background*.

a) b)

Figure 1: a) Range image cropped to bounding box. b) Manually enhanced label image, each color denotes a connected component determined by connected component labeling on the range image.

In order to assess the benefit of utilizing principle curves on TLS data, segmentation of phyto-elements has been performed manually on the basis of a previous connected component labeling step: For each of the obtained single tree images, the connected component labeling algorithm, as detailed in (Shapiro and Stockmann 2001), has been applied to the range values of the data tuples. Two neighboring pixels are defined to be *close* in 3D space and therefore connected pixels if the absolute difference of their range values does not exceed a predefined threshold ε. For the experiments, a threshold of $\varepsilon = 0.05\,m$ has been applied. Components representing a fragment of more than one branch due to a junction are split manually into separate components and a unique label l is assigned to each of them. Furthermore, the same label is assigned to disjoint components if they are representing the same branch according to

visual inspection. Very small components, which could not be assigned to a specific branch, have been eliminated. In that way, a unique label is determined for each separate phyto-element and propagated to the tuples of the pixels constituting the affected components as is demonstrated in figure 1b.

3.2 Experiment Setup

The 10 selected tree data sets have been prepared as explained in the previous section. Each input data set is treated as follows: For each unique label present in the current data set, a principal curve is computed for the corresponding 3D point subset. The point subset is obtained by selecting the 3D coordinates of all tuples where the label element matches the current label. Consequently, the result is a set of disjoint principal curves for each tree input data set. Linking the end points of the principal curve to attain a skeletal tree representation, as shown in figure 2b, could be performed automatically based on the segmented image (figure 1b), but has been conducted manually for simplicity. For the computation of the principal curves, an implementation in C++, which closely follows the prototype implementation provided in (Kégl 2000), has been utilized.

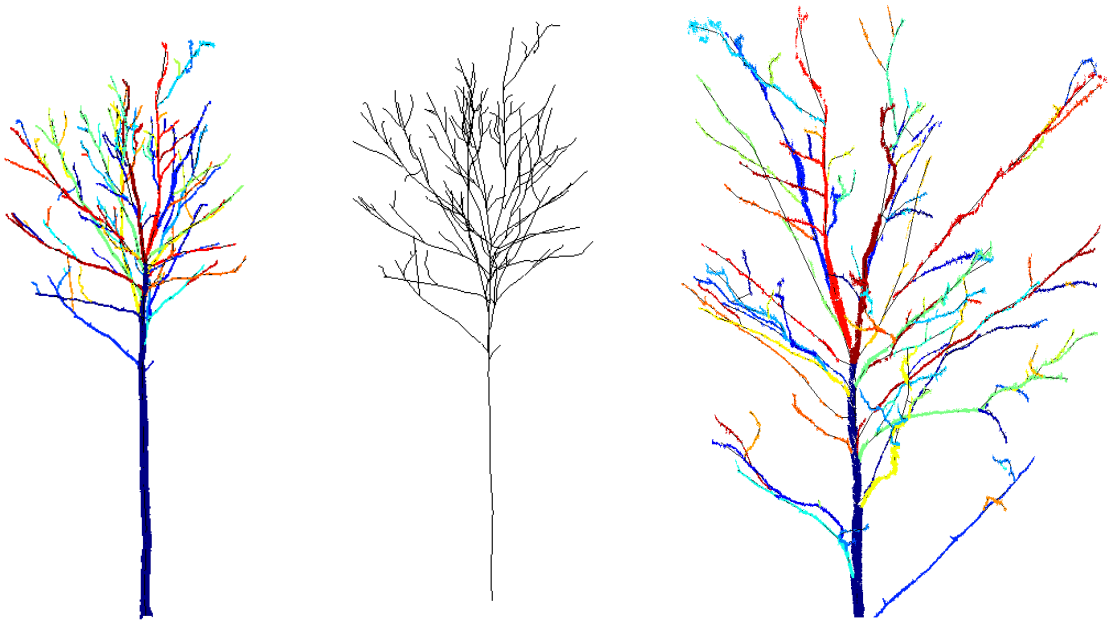

Figure 2: Resulting skeletal representations of tree ID 8. a) Tree skeleton with 3D points colored according to label. b) Skeleton of tree. c) Magnified crown with 3D points and skeleton.

4. Results

Figure 2 gives an impression of the retrieved skeletal structures with an overlay of the corresponding point sets. The result of the principal curve computation for each single tree trunk is presented in table 1. Retrieval of the trunk curve is most time intensive due to its comparably high number of involved points. Clearly, the number of 3D points has a great impact on the time necessary to compute the principal curve. In addition, more iterations are generally required by the algorithm if the number of outliers or the outlier's distance error is large. The mean distance error denotes the average Euclidean distance of a 3D point to its corresponding node of the polygonal line; therefore, it should approximate the diameter of the trunk.

Table 1: Results of experiments for point subsets representing trunks.

Tree ID	Curve comp. time [s]	Mean distance error [m]	Number of points	Distance from scanner [m]
1	3.322	0.0667	82757	16.34
2	32.262	0.0755	357058	7.89
3	20.312	0.0721	332869	8.00
4	7.784	0.0671	140413	12.92
5	42.385	0.0699	361463	7.26
6	5.086	0.0904	120028	14.13
7	13.510	0.0710	184115	11.61
8	17.144	0.0837	196224	12.47
9	4.961	0.0798	84848	20.57
10	5.070	0.0796	88623	19.11

Computation results for branches are summarized for each tree in table 2. All branches are completed in less than $0.5\,s$ for point sets ranging from 20 to 13141 points in size. Again, the computation is quite robust to improperly segmented points, i.e. outliers to the targeted 3D point set representing the branch. For entire trees, the mean distance error denotes the average Euclidean distance of a 3D point to its corresponding node of the polygonal line over all branches in the crown. If the points have been segmented properly, the mean distance error of branch curves is less $1\,cm$ on average. Curve segments exhibiting a larger error in comparison to pre- and succeeding segments indicate the presence of outliers, e.g. due to a new branch forking off or improper segmentation. In those cases, the mean distance error is significantly higher, i.e. in the magnitude of several decimeters. The shape of the principal curve is governed strongly by the point distribution and drawn to more dense clusters of 3D points. For this reason, if the number of outlier points is small, the principal curve can still be retrieved correctly with only little noise influence. As indicated in figure 2c, data gaps in a branch can be bridged as well. Although winding branches in the scans, caused by wind during data capture, cannot be traced in all detail, the general branch shape can still be retrieved. In fact, the resulting straight, unwinding principal curve is more plausible in those specific cases.

Judged on visual inspection, the obtained tree structures trace the original spatial branching structure very well. Clearly, the quality of the results strongly depends on the prior segmentation of phyto-elements and correctly linking of computed principle curves.

Table 2: Results of experiment for each tree, excluding their trunk subsets.

Tree ID	Number of curves	Total Time [s]	Mean distance error [m]	Std.dev. of distance error [m]	Total number of points in crown	Number of points in largest subset
1	52	1.132	0.0009	0.0025	37717	11707
2	36	2.654	0.0007	0.0008	86473	12877
3	45	3.450	0.0024	0.0018	127748	9528
4	22	0.702	0.0084	0.0018	17468	2693
5	29	2.558	0.0014	0.0024	74141	11800
6	36	0.780	0.0074	0.0016	29003	6525
7	54	1.996	0.0071	0.0013	73956	10890
8	105	4.805	0.0042	0.0047	141898	13141
9	102	2.013	0.0081	0.0017	66036	4069
10	83	2.105	0.0074	0.0097	64142	7954

5. Conclusion

In this paper, we have proposed a novel approach to retrieve skeletal structures from TLS data on the basis of principal curves. A principal curve is a compact summary of a point cloud's distribution as polygonal line. To our knowledge, principal curves have not been applied to TLS data sets before. For this reason, we have conducted experiments on a set of 10 selected tree point clouds to assess the feasibility and benefit of employing principal curves on TLS data. Since each phyto-element of a tree has to be computed by a separate principal curve, a prior segmentation has been necessary. Rather than introducing an arbitrary neighborhood on the 3D point cloud in form of a graph or voxel grid, we have exploited the implicit neighborhood structure of the scan's range image. A connected component labeling algorithm has been performed on the range data in the image matrix. Subsequently, this initial segmentation has been improved by splitting or joining components thus that a unique label has been assigned to each branch or trunk. For each label, a principle curve has been computed and the resulting polygonal lines of a single tree have been connected to a tree graph.

Our results show that the principal curve computation is fast, robust to noise and can also deal with data gaps, which makes it well suited for application on 3D data sets. Furthermore, exploiting the implicit neighborhood structure of the range image matrix clearly facilitates general processing of 3D data from a single scan. In this way, well-known image processing methods can be adapted and applied to TLS data. Consequently, we strive to devise a fully automatic algorithm for retrieval of a complete and faithful tree model on the basis of principle curves in the future.

Acknowledgements

The work presented here was funded by DFG (Deutsche Forschungsgemeinschaft) via the project PAK331. The Z+F scanner was kindly provided by the Institute for Traffic Planning and Road Traffic (Prof. Dr. Lippold). We would especially like to thank our project partners, Prof. Dr. Wagner and Mr. Wollmerstädt, for their support in data acquisition.

References

Binney, J. and Sukhatme, G. S., 2009. 3d Tree Reconstruction from Laser Range Data. In: *Proceedings of the IEEE International Conference on Robotics and Automation*, Los Angeles, Universtiy of Southern California: 1321– 1326.

Bucksch, A., 2011. Revealing the skeleton from imperfect point clouds. PhD Thesis, TU Delft, Delft, Netherlands.

Cheng, Z., Zhang, X., and Fourcaud, T., 2007. Tree Skeleton Extraction from a Single Range Image. In: *Proceedings of the International Symposium on Plant Growth Modeling and Applications*, Beijing, CAS: 274-281, 2006.

Côté, J.-F., Fournier, R. A. and Egli, R., 2011. An architectural model of trees to estimate forest structural attributes using terrestrial LiDAR. *Environmental Modelling & Software*, 26, 761–777.

Dai, M., Li, H. and Zhang, X., 2010. Tree Modeling through Range Image Segmentation and 3D Shape Analysis. *Advances in Neural Network Research & Applications*, 67, 413–422.

Dijkstra, E.W., 1959. A note on two problems in connexion with graphs. *Numerische Mathematik*, 1, 269–271.

Fischler, M.A. and Bolles, R.C., 1981. Random sample consensus: A paradigm for model fitting with applications to image analysis and automated cartography. *Communications of the ACM*, 24(6), 381–395.

Gatziolis, D., Popescu, S., Sheridan, R., and Ku, N.-W., 2010. Evaluation of terrestrial LiDAR technology for the development of local tree volume equations. In: B. Koch, G. Kändler, C. Teguem (Eds.). *Proceedings of SilviLaser 2010 - The 10th International Conference on LiDAR Applications for Assessing Forest Ecosystems*, Freiburg, Germany: 197–205.

Giannitrapani, R. and Murino, V., 1999. Three-Dimensional Skeleton extraction by point set contraction. In: *Proceedings of the International Conference on Image Processing*, Udine, Udine University: 565-569.

Gorte, B. and Pfeifer, N., 2004. Structuring Laser-scanned trees using 3d mathematical morphology. *International Archives of Photogrammetry and Remote Sensing*, 35(B5), 929–933.

Gorte, B. and Winterhalder, D., 2004. Reconstruction of laser-scanned trees using filter operations in the 3D raster domain. *International Archives of Photogrammetry, Remote Sensing and Spatial Information Sciences*, 36(8), 39–44.

Gorte, B., 2006. Skeletonization of Laser-Scanned Trees in the 3D Raster Domain. In: A. Abdul-Rahman, S. Zlatanova, V. Coors (Eds.). *Innovations in 3D Geo Information Systems*, Springer: 371–380.

Jolliffe, I. T., 2002. Principal Component Analysis. 2nd ed. Springer.

Kégl, B., 1999. Principal Curves: Learning, Design, and Applications. PhD Thesis, Concordia University, Montréal, Canada.

Kégl, B., 2000. Principal Curves. URL: http://www.iro.umontreal.ca/~kegl/research/pcurves/. Accessed: 22-Jun-2012.

Kégl, B., Krzyżak, A., Linder, T., and Zeger, K., 2000. Learning and design of principal curves. *IEEE Transactions on Pattern Analysis and Machine Intelligence*, 22(3), 281–297.

Livny, Y., Yan, F., Olson, M., Chen, B., Zhang, H., and El-Sana, J., 2010. Automatic Reconstrution of Tree Skeletal Structures from Point Clouds. *ACM Transactions on Graphics*, 29(6), Article No. 151.

Preuksakarn, C., Boudon, F., Ferraro, P., Durand, J.B., Nikimmaa, E., and Godin, C., 2010. Reconstructing Plant Architecture from 3D Laser scanner data. In: T. de Jong, D. Da Silva (Eds.). *Proceedings of the 6th International Workshop on Functional-Structural Plant Models*, Davis, University of California: 16-18.

Schilling, A., Schmidt, A. and Maas, H.-G., 2012. Tree Topology Representation from TLS Point Clouds Using Depth-First Search in Voxel Space. *Photogrammetric Engineering and Remote Sensing*, 78(4), 383–392.

Shapiro, L.G. and Stockmann, G.C., 2001. Binary Image Analysis. In: *Computer Vision*, Prentice Hall: 69–75.

Xu, H., Gossett, N. and Chen, B., 2007. Knowledge and Heuristic-based Modeling of Laser-Scanned Trees. *ACM Transactions on Graphics*, 26(4), Article No. 19.

Yan, D.-M., Wintz, J., Mourrain, B., Wang, W., Boudon, F. and Godin, C., 2009. Efficient and robust reconstruction of botanical structure from laser scanned data points. In: *Proceedings of the 11th IEEE International Conference on Computer-Aided Design and Computer Graphics*, Hong Kong, University of Hong Kong: 572–576.

Zoller+Fröhlich, 2009. Datasheet Z+F Imager 5006i. URL:http://www.zf-laser.com/Datenblatt_IMAGER5006i_E.pdf , Accessed: 03-Aug-2011.